Scientia Iranica B (2021) 28(3), 1259–1270

SCIENTIA IRANICA

Sharif University of Technology
Scientia Iranica
Transactions B: Mechanical Engineering
http://scientiairanica.sharif.edu

Experimental study of air injection effect on a surface to prevent ice formation

Y. Barzanouni[a,*], M. Gorji-Bandpy[a], and H. Basirat Tabrizi[b]

a. *Department of Mechanical Engineering,, Babol Noshirvani University of Technology (NIT), Babol, Mazandaran, 47148-71167, I.R. Iran.*
b. *Department of Mechanical Engineering, Amirkabir University of Technology (AUT), Tehran, 15875-4413, I.R. Iran.*

Received 17 August 2019; received in revised form 11 July 2020; accepted 22 August 2020

KEYWORDS
Ice-accretion;
Anti-icing system;
Icing wind tunnel;
Holes injection;
Design of experiments.

Abstract. In order to prevent ice-accretion on an airfoil surface, an experimental study was conducted to investigate the effect of injecting surrounding air from the surface into the main flow. For this purpose, holes were created at the leading edge of the airfoil. Five parameters of diameter, pitch, angle of position, hole arrangement, and the velocity of outlet flow from the holes were sought. Using the principles of experimental design using a two-level fractional factorial method, the required tests were designed and determined. Conducting tests, the results indicated the injection method significantly reduces the weight of ice accreted on the surface. The highest amount of ice mass reduction in experiments reached 85% of the ice mass accreted on the simple airfoil. The diameter and pitch of the holes had the greatest effect on reducing the mass of ice accreted on the surface, followed by the injection airflow rate and the angle of alignment. Therefore, the injection of air at a lower temperature than freezing point is as effective for ice accretion and saves energy rather than using hot-air injection. Moreover, the injected air from holes created a protective layer around the surface, which enhanced the process.

1. Introduction

Ice accretion on body and wing surfaces causes damage to the moving parts or disturbs the aerodynamic properties of the surface, which may lead to severe accidents, and, for example, the avoidance of flying under atmospheric conditions, which leads to ice accretion on the surface, is not always possible. Therefore, it is necessary to use anti-icing and deicing systems in the aircraft. Thomas et al. [1] stated some methods of deicing such as: i) use of freezing point depressants (the leading edges of the wings contain slots, through which ethylene glycol is expelled during flight), ii) surface deformation, iii) electro-thermal heaters or the passing of hot air onto the wing surface. When an aircraft is kept on the ground in cold moisture or snowy weather, ice accretion can be prevented by means of anti-icing fluid. The film on the wing, because of modification of the boundary layer, causes lift to be lost during takeoff. Research on the aerodynamic effect of de/anti-icing fluid can be found in [2–6]. Kohlman et al. [7] tested a glycol-exuding, porous leading-edge ice protection system. Results indicated that this method is a very effective means of preventing ice accretion or removing ice from wings. In addition, no significant drag penalty is associated with installation or operation. Hung et al. [8] used a graphite fiber-epoxy composite as the heating element, and a fiber glass-epoxy composite as the protecting layer with nickel foil contacting the end,

*. *Corresponding author. Tel.: +98-901-906-4445*
E-mail addresses: y.barzanoni@yahoo.com (Y. Barzanouni); gorji@nit.ac.ir (M. Gorji-Bandpy); hbasirat@aut.ac.ir (H. Basirat Tabrizi)

doi: 10.24200/sci.2020.54174.3628

made a highly electrically and thermally conductive heating element with a flexible structure to conform to an irregular surface. Petrenkov et al. [9,10] used a Pulse Electro-Thermal Deicer (PETD) to heat only a thin layer of interfacial ice to the melting point as fast as possible. By decreasing the heating duration, heated layer thickness was reduced. Hence, diffusion length and, consequently, thermal mass and thermal loss decreased. Palacios et al. [11] introduced a low power, non-thermal ultrasonic deicing system, which could be used for helicopter rotor blades. A flat plate and steel airfoil shapes were evaluated for this research. Ultrasonic transverse shear stresses at the interface of the accreted ice were generated, which de-bond thin ice layers as they form on the isotropic host. Overmayer et al. [12] used an ultrasonic deicing system in a structure representative of a rotorcraft blades leading edges, which was tested under impact icing and centrifugal environments (390 g). In addition, implementing the Finite Element Method (FEM), a bondline approach was used for a rotor blade leading edge. Power consumption was reduced by 85%, with respect to currently used electro-thermal deicing. Zeng and Song [13] investigated numerically and experimentally an ultrasonic deicing with sandwich transducers. Tests were performed on the aluminum and composite plate. They indicated that debonding time is much less than icing time. Super-cooled water droplets when on impact with the surface, before freezing, flow into crevices and move around the feature, and then freeze to clamp with the surface. Soltis et al. [14] examined the effects of surface characteristics on ice adhesion strength for titanium grade 2, titanium aluminum nitride, and titanium nitride coated on titanium grade 2. The ice adhesion strength of TiN and TiAlN coated on Ti2 was higher than the uncoated Ti2 substrate for similar surface roughness values. Understanding the ice adhesion strength for a given rotor-blade leading edge material is critical to the design erosion-resistant materials compatible with ice protective technologies. Further, Soltis et al. [15] evaluated the ice adhesion strength of erosion-resistant materials, titanium nitride and titanium aluminum nitride, experimentally, and compared the results to those of uncoated metallic materials used on a rotor-blade leading edge cap, such as stainless steel 430, inconel 625, and titanium grade 2. Their results indicated the impact ice adhesion strength of TiAlN and TiN were 30% and 35% higher than the average adhesion strength of uncoated materials. In addition, by minimizing the surface roughness of these coated materials, ice adhesion strength will decrease.

Low power electromechanical deicing systems, such as deicing systems based on piezoelectric actuators, are currently of more interest. Vibration generated by piezoelectric actuators at resonance frequencies causes the production of shear stress at the interface between the ice and the support or to produce tensile stress in the ice. Pommier-Budinger et al. [16] proposed a computational method for estimating voltages and currents of a piezoelectric deicing system to initiate cohesive fractures in the ice, or adhesive fractures at the ice/support interface. The method was based on modal analysis of the structure, which was validated through experiments. Their results indicated that in structures with bare aluminum alloys, the initiation of deicing is more likely due to tensile stress in the ice than shear stress at the interface between the ice and the support, especially at low frequencies. Budinger et al. [17] provided analytical and numerical models enabling better understanding of the main deicing mechanisms of resonant actuation systems. Different possible ice-shedding mechanisms involving cohesive and adhesive fractures were analyzed using an approach-combining modal, stress, and crack propagation analyses.

Ahn et al. [18] investigated, numerically and experimentally, ice accretion on an electro-thermal anti-icing system around a rotorcraft engine air intake. An Eulerian approach, DROP3D, and ICE3D modules of FENSAP-ICE were used to calculate the collection efficiency and ice shape on the surface. The experimental work was performed at the Centro Italiano Ricerche Aerospaziali (CIRA), Icing Wind Tunnel (IWT), with test section dimensions of 2.6 m $\times$ 3.8 m $\times$ 9.9 m.

Meng et al. [19] measured the surface temperatures of flat plate actuators under high voltage in quiescent air. Surface temperatures of the actuator were measured on a cylinder, in an icing wind tunnel for anti/deicing systems. An ice layer of 5 mm was removed completely over 150 s, after plasma actuating was on. A low power consumption of 13 kW/m^2 indicated good performance. The thermal effects of a Dielectric-Barrier-Discharge (DBD) plasma actuator and a conventional electrical film heater, as anti/deicing systems for aircraft, were compared by Liu et al. [20] in the Icing Research Tunnel of Iowa State University (i.e., ISU-IRT). NACA0012 airfoil was used with an AC-DBD plasma actuator and a conventional electrical film heater over the airfoil surface, and was tested under typical glaze icing conditions. For the same input power density, the AC-DBD plasma actuator and the electrical film heater indicated almost equivalent effectiveness in the prevention of icing over the airfoil surface. Wei et al. [21] proposed a "streamwise plasma heat knife" configuration based on a nanosecond pulsed surface dielectric barrier discharge for better anti-icing performance. This configuration prevents ice accretion on the leading edge, cuts ice into blocks, and has less influence on the aerodynamic characteristics of the original airfoil. Two ice conditions were selected and tested in an icing wind tunnel with a NACA0012 airfoil. The energy efficiency, that is, the ratio between heating energy and total

deposited energy during discharge, was shown to be $\eta_{\text{total}} = 21.6\%$.

Fitt and Pope [22] proposed hot-air injection to remove ice from a plate under icing conditions. The result is a nonlinear singular integral-differential equation, which was coupled with a convection/diffusion equation and the Stefan condition. Tabrizi and Keshock [23] used analytical analysis to investigate the effect of surface blowing as an antiicer. It was shown that for any upstream and cylinder conditions, the location of slots could be optimum, so that the anti-icing system has a maximum effect. Further, Tabrizi and Johanson [24] investigated experimentally to establish the effectiveness of surface blowing as anti-icing for aircraft. A circular cylinder with three span wise 4 by 0.014 inch slots located at the frontal surface of the cylinder was used. The effects of air blowing for single and multiple slots, as well as the effect of air injection rates on the ice accretion rate were investigated. Results confirmed the positive effect of injection on the reduction of ice accretion.

The proposed experimental research focuses on a new design for an anti-icing system using surrounding air with a temperature lower than freezing point for ice accretion in an airfoil. Hence, embedding aeration holes at the leading edge of the airfoil, based on the suggestion derived from the fractional factorial test.

2. Fractional factorial design

One of the most important factorial designs is the design with k factors, each having two levels. Such plans require $2 \times 2 \times \cdots \times 2 = 2^k$ observations that are called a 2^k factorial design. Along with an increasing number of factors, the number of runs needed to do the design increase more quickly than the available resources. Often, a smaller fraction of 2^k is favorable when increasing the number of factors. Consider a fraction of one-quarter of a 2^k factorial design. This design has 2^{k-2} runs and is called the one-quarter fraction of the 2^k design. The 2^{k-2} design may be constructed by first writing down a basic design consisting of the runs associated with a full factorial in $(k-2)$ factors, and then associating the two additional columns with appropriate chosen interactions involving the first $(k-2)$ factors [25].

In this study, there are five parameters, including "A", "B", "C", "D", and "E" that are velocity, hole diameter and pitch, angle between two rows and arrangement, respectively. A one-quarter fraction of the 2^k design has two generators, e.g. "ABD" and "ACE", called the generating relations, for the design. To make the design, first, one should write down the main design, which includes 8 runs for a full $2^{5-2} = 8$ design in "A", "B", and "C". Then, the remaining factors "D" and "E" should be added by associating their plus and minus levels with the plus and minus signs of the interactions "AB" and "AC", respectively, and the signs of "D" and "E" can be determined. This procedure is shown in Table 1. Table 1 shows the level of different factors during the test, e.g. in Run #8 all of them are running at their high level.

Table 1. A 2^{5-2} design with the defining relation I = ABD = ACE = BCDE.

	Basic design				
Run	**A**	**B**	**C**	**D = AB**	**E=AC**
1	-	-	-	+	+
2	+	-	-	-	-
3	-	+	-	-	+
4	+	+	-	+	-
5	-	-	+	+	-
6	+	-	+	-	+
7	-	+	+	-	-
8	+	+	+	+	+

3. Experimental set-up and methods

3.1. Wind tunnel

The wind tunnel is a suction open circuit tunnel, as shown in Figure 1. The dimensions of the test section are 30×30 cm, length is 60 cm, and the total length of the tunnel is 4.3 m. The maximum velocity in the test room is 35 and 28 ms^{-1}, without and with airfoil, respectively. Reynolds number is 430000 under test conditions at a temperature of -21°C, based on the airfoil chord. The power of the fan engine is 4 hp.

The wind tunnel is located inside an industrial refrigerator with the dimensions of $20 \times 30 \times 10$ m. The refrigerator temperature can be controlled between 0 to -40°C. The compressor of the cooling system ('Debica' brand) was made in Poland. Nozzles were manufactured in the Natural Fog Co. (R30S/10E model) for supplying the water droplets in the test. Data

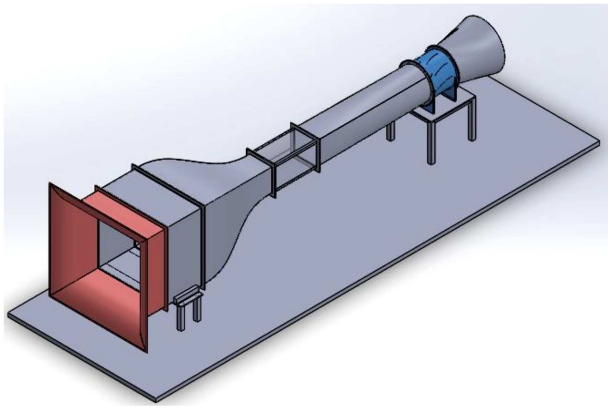

Figure 1. Wind tunnel.

Table 2. Specifications of CEM Dt-8920.

	Range	Resolution	Accuracy
Velocity (ms^{-1})	1–80	0.001	±2.5%
Pressure (Pa)	±5000	1	±0.3%
Temperature (°C)	0–50	0.1	±0.1

related to this nozzle, including the flow rate-pressure diagram, and diameters of the droplets at a pressure of 69 bars were used according to the manufacturing catalog. Measuring the flow rate of air inside the test section, a Pitot tube anemometer (CEM DT-8920 model made in Taiwan) was used. Table 2 shows the specifications of these instruments. To measure the flow rate required for each run, the TG1 brand rotameter flow meter (model LM-15G and LZM-15ZA) was used. The range of measurement was 1 to 10 and 0.1 to 1 m^3h^{-1}. The accuracy of each of these two models was ±4%. In order to increase the accuracy of reading, a grading ruler was used, along with the flow meter. The temperature control system was the "ELREHA. TAR 1820-2" controller made in Germany with a resolution of 0.1 degrees. Finally, the "A&D. GR200" scale, made in Japan, with a precision of ±0.001 grams was used for weighing the iced airfoil.

Figure 2 illustrates the schematic view of the test equipment in the refrigerator. The size of the refrigerator is large enough; therefore, the airflow does not affect the temperature.

3.2. Test procedures

The following procedure was used in this experimental study. This instruction is the same for Liquid-Water Content (LWC) distribution, repeatability, and basic tests.

1. First, the wind tunnel temperature should reach the test temperature. For this purpose, the refrigerator was switched on for about 5 hours before the start of testing until the temperature reaches the desired level;
2. Three airfoils (simple at both sides and a central drilled one) are mounted on their own stand and, by closing the screws of both sides, these three airfoils stick together completely and their surfaces become integrated. By connecting the compressed air hose to the air interface connected to the airfoil, it is possible to control the amount of desired air for each run using the relief valve and the rotameter;
3. The wind tunnel was illuminated. The speed was set in the test section according to the frequency-velocity diagram. All pieces of equipment were stored in the refrigerator and their temperature was the same as the air temperature of the refrigerator. However, after turning on the fan, ten minutes was allowed for the condition of the wind tunnel to become stable;
4. To prevent the freezing of the metal cap of the water nozzle and the water transfer hose, they were stored outside the refrigerator before starting the test. In order to transfer the nozzle into the refrigerator and install it in place, the water pump was first turned on and, then, the water nozzle was brought into the refrigerator and placed on the mesh of the nozzle of the wind tunnel, which was a predetermined

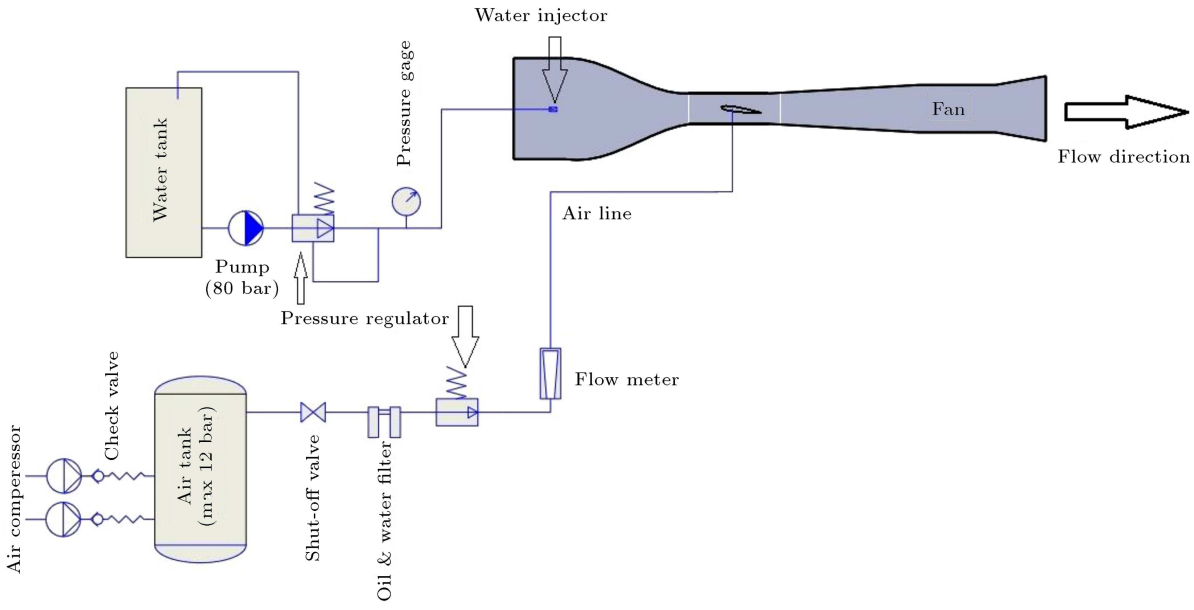

Figure 2. Schematic views of wind tunnel, water pump, and refrigerator.

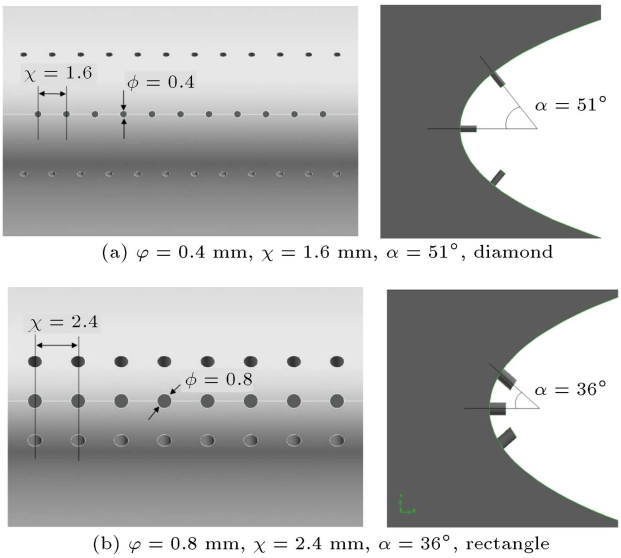

(a) $\varphi = 0.4$ mm, $\chi = 1.6$ mm, $\alpha = 51°$, diamond

(b) $\varphi = 0.8$ mm, $\chi = 2.4$ mm, $\alpha = 36°$, rectangle

Figure 3. Holes specification.

location. Immediately, the start time of the test was considered;

5. After three minutes, for all experiments, the pump was first turned off and the water nozzle removed from the refrigerator. Then, the wind tunnel fan was turned off and the ice-accreted airfoils removed from the wind tunnel;
6. Finally, the frozen part was evaluated in the refrigerator and, if necessary, photographs were taken of the part inside the refrigerator.

Figure 3 displays the specification of holes created at the leading edge. The right-hand side shapes are in line with the airfoil span, indicating the direction of the drilled holes.

Figure 4 displays the airfoils used in the experiment, as well as the drilled holes at the leading edge. The simple and slotted airfoils were used on the sides and in the middle, respectively.

To study the effect of blowing out on ice-accretion on the airfoil surface, the velocity of injection, the diameter and pitch of holes, the angles of the position of hole rows relative to the chord, and their arrangement, were investigated. The upstream conditions of the test, including the speed of the wind tunnel and the mean volume diameter of the droplets, were fixed in all experiments and equal to 21.2 ms^{-1} and 12 μm, respectively. Table 3 indicates the conditions and the number of each test.

Figure 4. Airfoil and holes embedded in the edge of the attack.

Tabrizi and Johanson [24] used slot injection with 0.014 in by 4 in, and the ratio of the maximum velocity of injection from the slot to the maximum and minimum of wind tunnel speed were reported as being 22.16 and 3.6, respectively. In this study, this ratio was in the range of 3.8-5.7 for the separated holes.

Tests 1 to 4 were performed on a simple airfoil to check the ice weight on a simple airfoil, as well as for checking the repeatability test. Thereafter, there are four experimental groups, each of which consists of eight tests carried out on the drilled airfoils. The first group has an inlet temperature of 252 K, an angle of attack of 4 degrees and a Liquid-Water Content (LWC) of 2.5 gm^{-3}, while the second group has a temperature of 252 K, an AOA of 8 degrees and an LWC of 3.5 gm^{-3}, and so on. Test conditions 1, 2, 3, and 4 are the same for groups 1, 2, 3, and 4, respectively. The simple airfoils are denoted with an "S. Airfoil" code, while the drilled airfoils are displayed with a number representing the holes characteristics. The first number is the diameter of the hole, which is either 4 (for 0.4 mm) or 8 (for 0.8 mm). The next two numbers are the pitch, that is, 16 (for 1.6 mm) or 24 (for 2.4 mm). The next two numbers indicate the angle of the holes position, which is 36 or 51 degrees, and finally, there is a letter indicating the rectangle or diamond shape.

3.3. Experimental calculation of the liquid-water content

In order to calculate the amount of LWC, the collection coefficient β should be first determined [26–28]. This coefficient is defined as the number of droplets that collide with the model. The collection coefficient along the surface will definitely change and its amount in the stagnation line is called β_0.

The collection coefficient is calculated according to Eq. (1) as suggested by Palacios et al. [27]:

$$\beta_0 = \frac{1.4(K_0 - 0.125)^{0.84}}{1 + 1.4(K - 0 - 0.125)^{0.84}}, \tag{1}$$

where K_0 represents the modified inertia parameter and is defined as:

$$K_0 = \frac{\lambda}{\lambda_{stockes}}(K - 0.125) + 0.125, \qquad K = \frac{\rho_w \delta^2 V}{18\mu_a C}.$$

Further, $\lambda/\lambda_{stockes}$ represents the ratio of the drag force imposed on the droplet from the flow to the drag force calculated from the Stokes law. This parameter is a function of the Reynolds number (in terms of the droplet diameter) and can be calculated as Eq. (2):

$$\frac{\lambda}{\lambda_{stockes}} = \frac{1}{0.8388 + 0.001483 Re_\delta + 0.1847\sqrt{Re_\delta}}. \tag{2}$$

Table 3. Test conditions.

	Test number	T_{air} (K)	AOA (deg)	LWC (gm^{-3})	V_{inj} (ms^{-1})	D (mm)	Pitch (mm)	A (deg)	Arrangement –	Airfoil code
	1	252	4	2.5	–	–	–	–	–	S. Airfoil
	2	252	8	3.5	–	–	–	–	–	S. Airfoil
	3	259	4	2.5	–	–	–	–	–	S. Airfoil
	4	259	8	3.5	–	–	–	–	–	S. Airfoil
Test group #1	5	252	4	2.5	80	0.4	1.6	51	Diamond	41651D
	6	252	4	2.5	120	0.4	1.6	36	Rectangle	41636R
	7	252	4	2.5	80	0.8	1.6	36	Diamond	81636D
	8	252	4	2.5	120	0.8	1.6	51	Rectangle	81651R
	9	252	4	2.5	80	0.4	2.4	51	Rectangle	42451R
	10	252	4	2.5	120	0.4	2.4	36	Diamond	42436D
	11	252	4	2.5	80	0.8	2.4	36	Rectangle	82436R
	12	252	4	2.5	120	0.8	2.4	51	Diamond	82451D
Test group #2	13	252	8	3.5	80	0.4	1.6	51	Diamond	41651D
	14	252	8	3.5	120	0.4	1.6	36	Rectangle	41636R
	15	252	8	3.5	80	0.8	1.6	36	Diamond	81636D
	16	252	8	3.5	120	0.8	1.6	51	Rectangle	81651R
	17	252	8	3.5	80	0.4	2.4	51	Rectangle	42451R
	18	252	8	3.5	120	0.4	2.4	36	Diamond	42436D
	19	252	8	3.5	80	0.8	2.4	36	Rectangle	82436R
	20	252	8	3.5	120	0.8	2.4	51	Diamond	82451D
Test group #3	21	259	4	2.5	80	0.4	1.6	51	Diamond	41651D
	22	259	4	2.5	120	0.4	1.6	36	Rectangle	41636R
	23	259	4	2.5	80	0.8	1.6	36	Diamond	81636D
	24	259	4	2.5	120	0.8	1.6	51	Rectangle	81651R
	25	259	4	2.5	80	0.4	2.4	51	Rectangle	42451R
	26	259	4	2.5	120	0.4	2.4	36	Diamond	42436D
	27	259	4	2.5	80	0.8	2.4	36	Rectangle	82436R
	28	259	4	2.5	120	0.8	2.4	51	Diamond	82451D
Test group #4	29	259	8	3.5	80	0.4	1.6	51	Diamond	41651D
	30	259	8	3.5	120	0.4	1.6	36	Rectangle	41636R
	31	259	8	3.5	80	0.8	1.6	36	Diamond	81636D
	32	259	8	3.5	120	0.8	1.6	51	Rectangle	81651R
	33	259	8	3.5	80	0.4	2.4	51	Rectangle	42451R
	34	259	8	3.5	120	0.4	2.4	36	Diamond	42436D
	35	259	8	3.5	80	0.8	2.4	36	Rectangle	82436R
	36	259	8	3.5	120	0.8	2.4	51	Diamond	82451D

The freezing fraction is the ratio of the number of droplets that freeze when colliding with the surface to the total droplets colliding with the surface. In order to calculate this parameter, the following relations first should be calculated with Eqs. (3) and (4):

$$\Phi = t_f - t_\infty - \frac{v^2}{2c_{p,w}}, \tag{3}$$

$$\theta = t_{surf} - t_\infty - \frac{v^2}{2c_{p,a}} + \frac{h_G}{h_c}\left[\frac{p_{w,surf} - p_{w,\infty}}{p_\infty}\right]\Lambda_v, \tag{4}$$

Φ and θ represent energy transfer from droplets and air, respectively.

The relative heat factor, b, can be defined as the ratio of the sensible heat absorbing capacity of the impinging water per unit of surface area to the unit convective heat-dissipating capacity of the same surface:

$$b = \frac{LWC.v.\beta_0.c_{p,w}}{h_c}. \tag{5}$$

Then, the freezing fraction can be defined with Eq. (6):

$$n = \frac{c_{p,w}}{\Lambda_f}\left[\Phi + \frac{\theta}{b}\right]. \tag{6}$$

Defining the mass flux as $\dot{m} = LWC.V.\beta_0$, the amount of ice thickness in the stagnation line can be calculated from Eq. (7):

$$\Delta = \frac{\dot{m}.\tau}{\rho_i} n_0. \tag{7}$$

Introducing the accumulation parameter, $A_c = LWC.V.\tau/(\rho_i.d)$, and using $\dot{m}$ in Eq. (7), the non-dimensionalized ice thickness can be calculated based on Eq. (8):

$$\Delta/d = n_{0,e}.A_c.\beta_0. \tag{8}$$

The experimental freezing fraction can be related to the analytical freezing fraction using Eq. (9):

$$n_{0,e} = 0.0184 + 1.107 n_{0,a}. \tag{9}$$

In order to determine the amount of LWC through the above relationships, the value of β_0 should first be determined. The first step is using Eqs. (1) to (4), which have a constant value because they are determined by applying upstream flow conditions. Then, in the second step, an initial value is given to the LWC and b, A_c, thus, freezing fraction, Eq. (6) and experimental freezing fraction, Eq. (9) are calculated. Finally, using Eq. (8), the ice thickness can be calculated. In the next step, this value is compared to the amount of ice thickness extracted from the test result, and the repetition stops if the difference between them is at the defined range, which is, in this study, 0.1 mm. Otherwise, there is a return to the second step, the LWC value is added, and steps 2 and 3 are repeated.

Figure 5. Icing grid used to evaluate the cloud uniformity and its accreted ice.

References [29–31] used a grid to determine where the spray from each spray bar ended in the test section. In this study, a 28 by 28 cm steel grid was installed on the stand of the airfoil and placed in the middle of the test section as shown in Figure 5.

This caused the entire test section to be covered. The grid has 1.5 cm vertical and horizontal spacing. Then, according to the six steps as mentioned earlier, ice accretion on the mesh can be examined. Here, this is a quality evaluation and cannot by any means be exact. The shape of the ice cross-section was depicted on the paper and plotted. Then, the resulting curve was converted to a set of data.

4. Results and discussion

Experiments were conducted four times to confirm repeatability under test conditions, as described in Table 3. Figures 6 and 7 depict for test nos. 1 and 2, respectively, and Table 4 shows for test nos. 1 to 4. Table 4 represents the magnitude of the errors. To calculate the error, the average thickness (by eliminating the amount of noise) is considered as the reference. It should be noted this method of drawing the curve is only possible for simple airfoils due to the fragile nature of the ice accreted on the airfoil. As observed, the repeatability of the shape is acceptable in various runs.

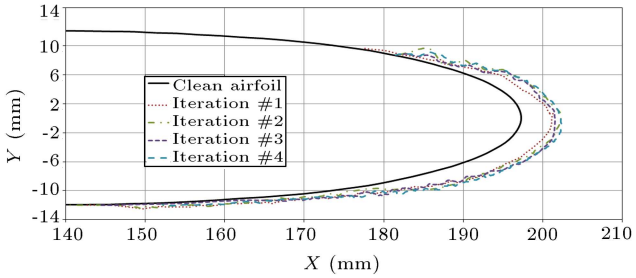

Figure 6. Repeatability of ice accretion on the simple airfoil (Test no. 1, Table 3).

Table 4. Ice thickness and error value relative to the average thickness in repeatability tests.

Iteration	Test number #1		Test number #2		Test number #3		Test number #4	
	Thickness mm	Error (%)	Thickness (mm)	Error (%)	Thickness (mm)	Error (%)	Thickness (mm)	Error (%)
1	4.99	–5.13	6.035	–10.44	5.229	–15.22	5.664	–7.38
2	4.96	–4.49	5.564	–1.82	4.284	5.60	5.165	2.09
3	4.29	9.62	4.794	12.26	4.309	5.06	4.996	5.29
4	3.79	20.15	3.380	38.14	4.332	4.56	3.852	26.979
Average	4.75		5.46		4.53		5.27	

Figures 8 and 9 illustrate the ice weight plotted in each run. The horizontal axis represents the test code, as shown in Table 3. This code is common for each group of experiments, as it shows the specification of holes created at the leading edge.

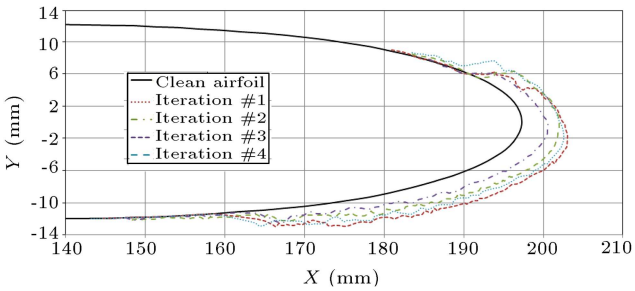

Figure 7. Repeatability of ice accretion on the simple airfoil (Test no. 2, Table 3).

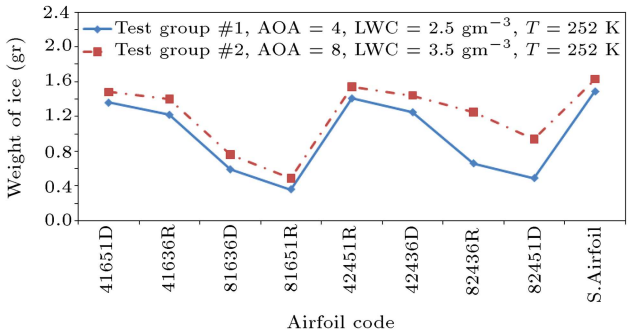

Figure 8. Ice mass diagram in terms of the airfoil code.

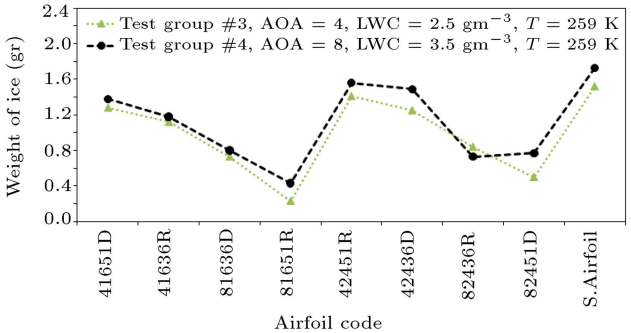

Figure 9. Ice mass diagram in terms of the airfoil code.

In general, the amount of ice formed for the AOA of 8 degrees is greater than that of 4 degrees. Increase in the angle of attack increases the ice weight, which can be related to an increase in the surface against the flow and a reduction of the effect of the upper row holes. The trend of mass variation is quite similar for both figures and there is negligible difference.

Table 5 introduces the maximum and minimum percentages of reduction of ice mass accreted on the drilled airfoil, compared to the simple airfoil. As shown in Table 5, the maximum reduction value is obtained for a given drilled airfoil and a similar process is observed in the case of minimum reduction. The maximum reduction in the ice mass in the presence of air injection from the holes reached 85%, which is significant. As shown in Figure 10, it can be expected that during an increase in test time, the formed ice thickens, breaks, and completely separates from the surface due to the coming flow force on its surface.

The amount of ice-accreted in Figure 11 is 1.25 gr. Due to the diameter of the hole size, which is 0.4 mm, and the higher speed of injection flow, 120 ms^{-1}, the effect of the injected flow fails to dominate ice-accretion, which only effects injection flow. This effect is intensified when the velocity of the injected flow is at its lowest limit.

Figure 12 indicates the ice-accreted in Test no. 12. The speed of injected flow and hole diameters are at their highest level, here, 0.8 mm. The pitch size of the holes is higher, which is the only difference in size, as compared to Figure 10. This incremental pitch caused

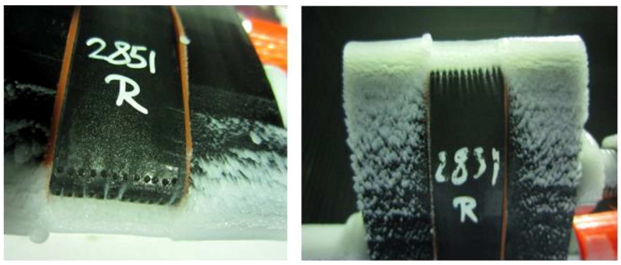

Figure 10. Ice accreted on the airfoil for Test no. 24. AOA = 4°, LWC = 2.5 gm^{-3}, T = 259 K, 81651R.

Table 5. Maximum and minimum blowing effect on the ice accretion.

	Max reduction (%)	Airfoil code	Min reduction (%)	Airfoil code
Test group #1	75.84	81651R	5.37	42451R
Test group #2	69.94	81651R	5.52	42451R
Test group #3	84.87	81651R	7.24	42451R
Test group #4	75.14	81651R	9.83	42451R

Table 6. Effect of each factor.

	Test group #1	Test group #2	Test group #3	Test group #4
V	4.40	6.44	11.87	–
φ	94.58	79.47	83.55	85.84
χ	0.52	9.10	3.81	6.55
α	0.43	–	–	–
$\varphi \times \chi$	–	3.71	–	–

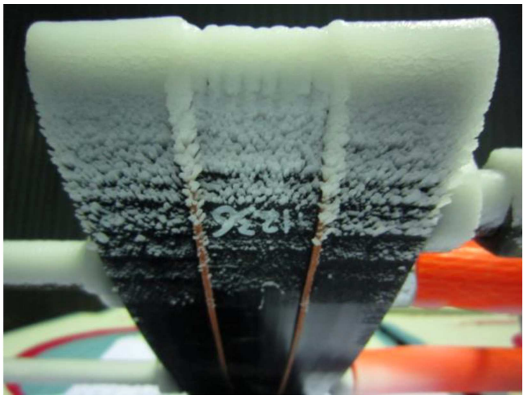

Figure 11. Ice accreted on the airfoil for Test no. 10. AOA = 4°, LWC = 2.5 gm^{-3}, T = 252 K, 42436D.

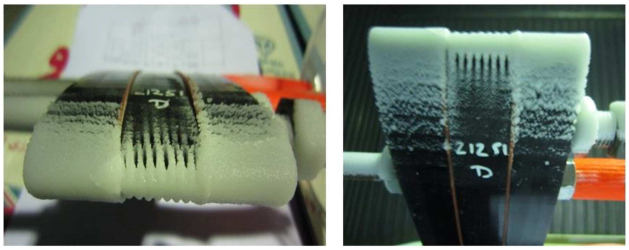

Figure 12. Ice accreted on the airfoil for Test no. 12. AOA = 4°, LWC = 2.5 gm^{-3}, T = 252 K, 82451D.

the protective layer of the air to weaken around the airfoil and, thus, the accreted ice is different in terms of the shape, which can be observed from the two shown figures.

In order to investigate which parameters play the greater role on ice-accretion on the surface, an analysis was performed based on obtained data from the Minitab software. Minitab offers five types of design: screening, factorial, response surface, mixture, and Taguchi. The steps are followed in Minitab to create, analyze, and visualize a designed experiment that is similar for all types. After once performing the experiment and entering the results, Minitab provides several analytical tools and graph tools to help understand the results [32]. Performing appropriate statistical operations on the data, the relationships between important factors in each series of experiments in the form of the following formulas were obtained from Eq. (10).

$$m^{2}_{\text{ice,Test Group\#1}} = 3.3937 - 0.007756V - 3.5947\varphi + 0.1334\chi + 0.006487\alpha,$$

$$\frac{m^{2.4-1}_{\text{ice,Test Group \#2}}}{2.4 \times 1.09123^{2.4-1}} = 2.103 - 0.00443V - 3.238\varphi - 0.241\chi + 0.841\varphi\chi,$$

$$m^{1.58}_{\text{ice,Test Group\#3}} = 3.1263 - 0.009463V - 2.51051\varphi + 2.6811\chi - 0.005928\alpha,$$

$$m^{1.58}_{\text{ice,Test Group\#4}} = 2.4514 - 3.75\varphi + 0.518\chi. \quad (10)$$

Table 6 describes the percentage of contribution of each factor in the model. From this table, the ratio of the effect of different factors relative to each other can be determined. It is worth noting that this ratio is sometimes very high, indicating even some of the factors identified can be neglected.

In all four experimental groups, the diameter of the holes is the most important factor. Based on Table 6, the holes diameter has a minimum effect of 80%. In an experiment with an AOA of 4 degrees, the speed of blowing out flow and the pitch, followed by the angle of the arrangement are the most important factors. While at AOA of 8 degrees, the pitch is the most important factor after diameter. Another

common point of all outputs is the arrangement of the holes does not have any effect on the amount of ice mass and can be neglected for a series of supplementary experiments or optimizations.

5. Conclusion

Different deicing and anti-icing systems have been studied to prevent accidents related to freezing and each has its advantages and disadvantages depending on their performance. In the method presented in this study, using the surrounding air, and injecting through the drilled holes on the surface was proposed to counter the phenomenon of ice accretion on the surface. Under different upstream conditions, the injected air velocity, holes diameter, pitch of the holes, their position angles, and arrangement, were investigated. Using a two-level fractional factorial method, the required tests were designed and determined. Results indicated hole diameters and their pitches could be considered important and effective factors in reducing ice mass in all experiments. The larger the diameter and the smaller the pitch, the lower the amount of ice-accretion on the surface. Further, the velocity of the injected flow and the angle of the position were introduced as the next effective factors. However, almost no interaction was observed between important factors, indicating that the factors are independent of each other and have no effect on other performance. This method could reduce up to 85% of the ice weight accreted on the surface. Specifically, the amount of accreted ice reduced significantly if the temperature of the injected air was greater than zero. However, using hot-air ejection from the hole will get better results. Nevertheless, using the surrounding air injection, as undertaken in this research, indicates its effectiveness against ice accretion and also saves energy.

Acknowledgments

The authors would like to thank the Department of Mechanical Engineering and Office of Research of Babol Noshirvani University of Technology, for supporting this project. This project was undertaken using the research grant provided by Babol Noshirvani University of Technology, only.

Nomenclature

A_c	Accumulation parameter, dimensionless
AC-DBD	Alternating Current Dielectric Barrier Discharge
AOA	Angle of Attack, degree
b	Relative heat factor, dimensionless
c	Airfoil chord (m)
c_p	Specific heat ($Jkg^{-1}K^{-1}$)
d	Cylinder diameter or twice the leading-edge radius of airfoil, m
h_c	Convective heat-transfer coefficient ($Wm^{-2}K^{-1}$)
h_G	Gas-phase mass-transfer coefficient ($gm^{-1}s^{-1}$)
k	Thermal conductivity ($Wm^{-1}K^{-1}$)
K	Inertia parameter, dimensionless
K_0	Modified inertia parameter, dimensionless
LWC	Liquid-Water Content (gm^{-3})
MVD	Water droplet median volume diameter (μm)
n	Freezing fraction, dimensionless
n_a	Freezing fraction calculated using Messinger analysis, dimensionless
n_e	Freezing fraction from leading-edge ice thickness, dimensionless
p	Static pressure (Nm^{-2})
p_w	Vapor pressure of water (Nm^{-2})
t	Temperature (°C)
T	Absolute temperature (K)
V	Free-stream velocity of air, air injection velocity from holes (ms^{-1})
α	Angle of holes position
β_0	Collection efficiency at stagnation line, dimensionless
δ	Water droplet median volume diameter (μm)
Δ	Ice thickness at stagnation line (cm)
θ	Air energy transfer parameter (°C)
λ	Water droplet range (m)
$\lambda_{stockes}$	Water droplet range if stokes law applies (m)
Λ_f	Latent heat of freezing of water (Jkg^{-1})
Λ_v	Latent heat of evaporation of water (Jkg^{-1})
μ	Viscosity ($gm^{-1}s^{-1}$)
ρ	Density (kgm^{-3})
τ	Time (sec)
χ	Pitch of holes
φ	Diameter of the holes (m)
Φ	Water droplet energy transfer parameter (°C)

Subscripts

a	Air
f	Freezing point of water
i	Ice
$s, surf$	Icing surface
w	Water
∞	Atmosphere condition

References

1. Thomas, S.K., Cassoni, R.P., and MacArthur, C.D. "Aircraft anti-icing and de-icing techniques and modeling", *Journal of Aircraft*, **33**(5), pp. 841–854 (1996).
2. Broeren, A.P., Lee, S., and Clark, C. "Aerodynamic effects of anti-icing fluids on a thin high-performance wing section", *Journal of Aircraft*, **53**(2), pp. 451–462 (2015).
3. Hill, E.G. and Zierten, T.A. "Aerodynamic effects of aircraft ground deicing/anti-icing fluids", *Journal of Aircraft*, **30**(1), pp. 24–34 (1993).
4. Koivisto, P., Soinne, E., and Kivekäs, J. "Anti-icing fluid secondary wave and its role in lift loss during takeoff", *Journal of Aircraft*, **55**(6), pp. 2298–2306 (Nov. 2018).
5. Perron, E., Louchez, P.R., and Laforte, J.L. "Introductory analysis of boundary-layer development on de/anti-icing fluid", *Journal of Aircraft*, **33**(1), pp. 74–80 (1996).
6. Van Hengst, J. "Aerodynamic effects of ground de/anti-icing fluids on Fokker 50 and Fokker 100", *Journal of Aircraft*, **30**(1), pp. 35–40 (1993).
7. Kohlman, D.L., Schweikhardt, W.G., and Evanich, P. "Icing-tunnel tests of a glycol-exuding, porous leading-edge ice protection system", *Journal of Aircraft*, **19**(8), pp. 647–654 (1982).
8. Hung, C.-C., Dillehay, M.E., and Stahl, M. "A heater made from graphite composite material for potential deicing application", *Journal of Aircraft*, **24**(10), pp. 725–730 (1987).
9. Petrenko, V.F., Higa, M., Starostin, M., et al. "Pulse electrothermal de-icing", in *The Thirteenth International Offshore and Polar Engineering Conference*, International Society of Offshore and Polar Engineers (2003).
10. Petrenko, V.F., Sullivan, C.R., Kozlyuk, V., et al. "Pulse electro-thermal de-icer (PETD)", *Cold Regions Science and Technology*, **65**(1), pp. 70–78 (2011).
11. Palacios, J., Smith, E., Rose, J., et al. "Instantaneous de-icing of freezer ice via ultrasonic actuation", *AIAA Journal*, **49**(6), pp. 1158–1167 (2011).
12. Overmeyer, A., Palacios, J., and Smith, E. "Ultrasonic de-icing bondline design and rotor ice testing", *AIAA Journal*, **51**(12), pp. 2965–2976 (2013).
13. Zeng, J. and Song, B. "Research on experiment and numerical simulation of ultrasonic de-icing for wind turbine blades", *Renewable Energy*, **113**, pp. 706–712 (2017).
14. Soltis, J., Palacios, J., Eden, T., et al. "Ice adhesion mechanisms of erosion-resistant coatings", *AIAA Journal*, **53**(3), pp. 654–662 (2014).
15. Soltis, J., Palacios, J., Eden, T., et al. "Evaluation of ice-adhesion strength on erosion-resistant materials", *AIAA Journal*, **53**(7), pp. 1825–1835 (2014).
16. Pommier-Budinger, V., Budinger, M., Rouset, P., et al. "Electromechanical resonant ice protection systems: initiation of fractures with piezoelectric actuators", *AIAA Journal*, **56**(11), pp. 4400–4411 (2018).
17. Budinger, M., Pommier-Budinger, V., Bennani, L., et al. "Electromechanical resonant ice protection systems: analysis of fracture propagation mechanisms", *AIAA Journal*, **56**(11), pp. 4412–4422 (2018).
18. Ahn, G.B., Jung, K.Y., Myong, R.S., et al. "Numerical and experimental investigation of ice accretion on rotorcraft engine air intake", *Journal of Aircraft*, **52**(3), pp. 903–909 (2015).
19. Meng, X., Cai, J., Tian, Y., et al. "Experimental study of anti-icing and deicing on a cylinder by DBD plasma actuation", in *47th AIAA Plasmadynamics and Lasers Conference*, American Institute of Aeronautics and Astronautics (2016).
20. Liu, Y., Kolbakir, C., and Hu, H. "A comparison study on AC-DBD plasma and electrical heating for aircraft icing mitigation", in *2018 AIAA Aerospace Sciences Meeting*, American Institute of Aeronautics and Astronautics (2018).
21. Wei, B., Wu, Y., Liang, H., et al. "SDBD based plasma anti-icing: a stream-wise plasma heat knife configuration and criteria energy analysis", *International Journal of Heat and Mass Transfer*, **138**, pp. 163-172 (2019).
22. Fitt, A.D. and Pope, M.P. "De-icing by slot injection", *Acta Mechanica*, **147**(1), pp. 73–86 (2001).
23. Tabrizi, A.H. and Keshock, E.G. "Modeling of surface blowing as an anti-icing technique for aircraft surfaces", *Journal of Aircraft*, **25**(4), pp. 343–348 (1988).
24. Tabrizi, A.H. and Johnson, W.S. "Surface-blowing anti-icing technique for aircraft surfaces", *Journal of Aircraft*, **26**(4), pp. 354–359 (1989).
25. Montgomery, D.C., *Design and Analysis of Experiments*, Sixth Ed., John Wiley & Sons (2007).
26. Han, Y., Palacios, J., and Schmitz, S. "Scaled ice accretion experiments on a rotating wind turbine blade", *Journal of Wind Engineering and Industrial Aerodynamics*, **109**, pp. 55–67 (2012).
27. Palacios, J.L., Han, Y., Brouwers, E.W., et al. "Icing environment rotor test stand liquid water content

measurement procedures and ice shape correlation", *Journal of the American Helicopter Society*, **57**(2), pp. 29–40 (2012).

28. Tsao, J.-C., Vargas, M., and Kreeger, R. "Experimental evaluation of stagnation point collection efficiency of the NACA 0012 swept wing tip", in *1st AIAA Atmospheric and Space Environments Conference* (2010).

29. IDE, R. "Liquid water content and droplet size calibration of the NASA Lewis icing research tunnel", in *28th Aerospace Sciences Meeting* (1990).

30. Ide, R. and Oldenburg, J. "Icing cloud calibration of the NASA Glenn icing research Tunnel", in *39th Aerospace Sciences Meeting and Exhibit* (2001).

31. Ide, R.F. and Sheldon, D.W. *2006 Icing Cloud Calibration of the NASA Glenn Icing Research Tunnel*, National Aeronautics and Space Administration (2008).

32. Minitab, L. "Designing an experiment", Available from: https://support.minitab.com/en-us/minitab/18/getting-started/designing-an-experiment/ (2019).

Biographies

Yasser Barzanouni obtained his BS degree in Mechanical Engineering from Guilan University (Rasht, Iran) in 2007, and his MS degree in Mechanical Engineering from Amir Kabir University of Technology (Tehran, Iran) in 2011, and a PhD degree in Mechanical Engineering from Babol Noshirvani University of Technology (NIT), Babol, Mazandaran, Iran, in 2021. His research interests include fluid mechanics, frost formation and ice accretion, fan design and numerical simulation.

Mofid Gorji-Bandpy received his BS and MS degrees in Mechanical Engineering from Tehran University of Technology in 1976 and 1978, respectively, and a PhD degree in Mechanical Engineering from the University of Wales, England. He is currently a Full Professor of Mechanical Engineering at Babol Noshirvani University of Technology (NIT), Babol, Mazandaran, Iran. His research interests include fluid mechanics, turbomachinery, renewable energy, water distribution networks, mechanics and thermodynamics of propulsion systems and internal combustion chambers.

Hassan Basirat Tabrizi is Professor Emeritus in the Department of Mechanical Engineering at Amirkabir University of Technology (AUT), Tehran, Iran. His current research interests include the area of thermal-fluid at AUT, and also collaborative research with the Faculty of Mechanical Engineering of Jundi-Shapor University of Technology, Dezful, Iran.